

**Scaling properties of proton and anti-proton production
in $\sqrt{s_{NN}} = 200$ GeV Au+Au collisions**

S.S. Adler,⁵ S. Afanasiev,¹⁷ C. Aidala,⁵ N.N. Ajitanand,⁴³ Y. Akiba,^{20,38} J. Alexander,⁴³ R. Amirkas,¹² L. Aphecetche,⁴⁵ S.H. Aronson,⁵ R. Auerbeck,⁴⁴ T.C. Awes,³⁵ R. Azmoun,⁴⁴ V. Babintsev,¹⁵ A. Baldisseri,¹⁰ K.N. Barish,⁶ P.D. Barnes,²⁷ B. Bassalleck,³³ S. Bathe,³⁰ S. Batsouli,⁹ V. Baublis,³⁷ A. Bazilevsky,^{39,15} S. Belikov,^{16,15} Y. Berdnikov,⁴⁰ S. Bhagavatula,¹⁶ J.G. Boissevain,²⁷ H. Borel,¹⁰ S. Borenstein,²⁵ M.L. Brooks,²⁷ D.S. Brown,³⁴ N. Bruner,³³ D. Bucher,³⁰ H. Buesching,³⁰ V. Bumazhnov,¹⁵ G. Bunce,^{5,39} J.M. Burward-Hoy,^{26,44} S. Butsyk,⁴⁴ X. Camard,⁴⁵ J.-S. Chai,¹⁸ P. Chand,⁴ W.C. Chang,² S. Chernichenko,¹⁵ C.Y. Chi,⁹ J. Chiba,²⁰ M. Chiu,⁹ I.J. Choi,⁵² J. Choi,¹⁹ R.K. Choudhury,⁴ T. Chujo,⁵ V. Cianciolo,³⁵ Y. Cobigo,¹⁰ B.A. Cole,⁹ P. Constantin,¹⁶ D.G. d'Enterria,⁴⁵ G. David,⁵ H. Delagrange,⁴⁵ A. Denisov,¹⁵ A. Deshpande,³⁹ E.J. Desmond,⁵ O. Dietzsch,⁴¹ O. Drapier,²⁵ A. Drees,⁴⁴ R. du Rietz,²⁹ A. Durum,¹⁵ D. Dutta,⁴ Y.V. Efremenko,³⁵ K. El Chenawi,⁴⁹ A. Enokizono,¹⁴ H. En'yo,^{38,39} S. Esumi,⁴⁸ L. Ewell,⁵ D.E. Fields,^{33,39} F. Fleuret,²⁵ S.L. Fokin,²³ B.D. Fox,³⁹ Z. Fraenkel,⁵¹ J.E. Frantz,⁹ A. Franz,⁵ A.D. Frawley,¹² S.-Y. Fung,⁶ S. Garpman,²⁹ * T.K. Ghosh,⁴⁹ A. Glenn,⁴⁶ G. Gogiberidze,⁴⁶ M. Gonin,²⁵ J. Gosset,¹⁰ Y. Goto,³⁹ R. Granier de Cassagnac,²⁵ N. Grau,¹⁶ S.V. Greene,⁴⁹ M. Grosse Perdekamp,³⁹ W. Guryn,⁵ H.-Å. Gustafsson,²⁹ T. Hachiya,¹⁴ J.S. Haggerty,⁵ H. Hamagaki,⁸ A.G. Hansen,²⁷ E.P. Hartouni,²⁶ M. Harvey,⁵ R. Hayano,⁸ X. He,¹³ M. Heffner,²⁶ T.K. Hemmick,⁴⁴ J.M. Heuser,⁴⁴ M. Hibino,⁵⁰ J.C. Hill,¹⁶ W. Holzmann,⁴³ K. Homma,¹⁴ B. Hong,²² A. Hoover,³⁴ T. Ichihara,^{38,39} V.V. Ikonnikov,²³ K. Imai,^{24,38} D. Isenhower,¹ M. Ishihara,³⁸ M. Issah,⁴³ A. Isupov,¹⁷ B.V. Jacak,⁴⁴ W.Y. Jang,²² Y. Jeong,¹⁹ J. Jia,⁴⁴ O. Jinnouchi,³⁸ B.M. Johnson,⁵ S.C. Johnson,²⁶ K.S. Joo,³¹ D. Jouan,³⁶ S. Kametani,^{8,50} N. Kamihara,^{47,38} J.H. Kang,⁵² S.S. Kapoor,⁴ K. Katou,⁵⁰ S. Kelly,⁹ B. Khachaturov,⁵¹ A. Khanzadeev,³⁷ J. Kikuchi,⁵⁰ D.H. Kim,³¹ D.J. Kim,⁵² D.W. Kim,¹⁹ E. Kim,⁴² G.-B. Kim,²⁵ H.J. Kim,⁵² E. Kistenev,⁵ A. Kiyomichi,⁴⁸ K. Kiyoyama,³² C. Klein-Boesing,³⁰ H. Kobayashi,^{38,39} L. Kochenda,³⁷ V. Kochetkov,¹⁵ D. Koehler,³³ T. Kohama,¹⁴ M. Kopytine,⁴⁴ D. Kotchetkov,⁶ A. Kozlov,⁵¹ P.J. Kroon,⁵ C.H. Kuberg,^{1,27} K. Kurita,³⁹ Y. Kuroki,⁴⁸ M.J. Kweon,²² Y. Kwon,⁵² G.S. Kyle,³⁴ R. Lacey,⁴³ V. Ladygin,¹⁷ J.G. Lajoie,¹⁶ A. Lebedev,^{16,23} S. Leckey,⁴⁴ D.M. Lee,²⁷ S. Lee,¹⁹ M.J. Leitch,²⁷ X.H. Li,⁶ H. Lim,⁴² A. Litvinenko,¹⁷ M.X. Liu,²⁷ Y. Liu,³⁶ C.F. Maguire,⁴⁹ Y.I. Makdisi,⁵ A. Malakhov,¹⁷ V.I. Manko,²³ Y. Mao,^{7,38} G. Martinez,⁴⁵ M.D. Marx,⁴⁴ H. Masui,⁴⁸ F. Matathias,⁴⁴ T. Matsumoto,^{8,50} P.L. McGaughey,²⁷ E. Melnikov,¹⁵ F. Messer,⁴⁴ Y. Miake,⁴⁸ J. Milan,⁴³ T.E. Miller,⁴⁹ A. Milov,^{44,51} S. Mioduszewski,⁵ R.E. Mischke,²⁷ G.C. Mishra,¹³ J.T. Mitchell,⁵ A.K. Mohanty,⁴ D.P. Morrison,⁵ J.M. Moss,²⁷ F. Mühlbacher,⁴⁴ D. Mukhopadhyay,⁵¹ M. Muniruzzaman,⁶ J. Murata,^{38,39} S. Nagamiya,²⁰ J.L. Nagle,⁹ T. Nakamura,¹⁴ B.K. Nandi,⁶ M. Nara,⁴⁸ J. Newby,⁴⁶ P. Nilsson,²⁹ A.S. Nyanin,²³ J. Nystrand,²⁹ E. O'Brien,⁵ C.A. Ogilvie,¹⁶ H. Ohnishi,^{5,38} I.D. Ojha,^{49,3} K. Okada,³⁸ M. Ono,⁴⁸ V. Onuchin,¹⁵ A. Oskarsson,²⁹ I. Otterlund,²⁹ K. Oyama,⁸ K. Ozawa,⁸ D. Pal,⁵¹ A.P.T. Palounek,²⁷ V.S. Pantuev,⁴⁴ V. Papavassiliou,³⁴ J. Park,⁴² A. Parmar,³³ S.F. Pate,³⁴ T. Peitzmann,³⁰ J.-C. Peng,²⁷ V. Peresedov,¹⁷ C. Pinkenburg,⁵ R.P. Pisani,⁵ F. Plasil,³⁵ M.L. Purschke,⁵ A.K. Purwar,⁴⁴ J. Rak,¹⁶ I. Ravinovich,⁵¹ K.F. Read,^{35,46} M. Reuter,⁴⁴ K. Reygers,³⁰ V. Riabov,^{37,40} Y. Riabov,³⁷ G. Roche,²⁸ A. Romana,²⁵ M. Rosati,¹⁶ P. Rosnet,²⁸ S.S. Ryu,⁵² M.E. Sadler,¹ N. Saito,^{38,39} T. Sakaguchi,^{8,50} M. Sakai,³² S. Sakai,⁴⁸ V. Samsonov,³⁷ L. Sanfratello,³³ R. Santo,³⁰ H.D. Sato,^{24,38} S. Sato,^{5,48} S. Sawada,²⁰ Y. Schutz,⁴⁵ V. Semenov,¹⁵ R. Seto,⁶ M.R. Shaw,^{1,27} T.K. Shea,⁵ T.-A. Shibata,^{47,38} K. Shigaki,^{14,20} T. Shiina,²⁷ C.L. Silva,⁴¹ D. Silvermyr,^{27,29} K.S. Sim,²² C.P. Singh,³ V. Singh,³ M. Sivertz,⁵ A. Soldatov,¹⁵ R.A. Soltz,²⁶ W.E. Sondheim,²⁷ S.P. Sorensen,⁴⁶ I.V. Sourikova,⁵ F. Staley,¹⁰ P.W. Stankus,³⁵ E. Stenlund,²⁹ M. Stepanov,³⁴ A. Ster,²¹ S.P. Stoll,⁵ T. Sugitate,¹⁴ J.P. Sullivan,²⁷ E.M. Takagui,⁴¹ A. Taketani,^{38,39} M. Tamai,⁵⁰ K.H. Tanaka,²⁰ Y. Tanaka,³² K. Tanida,³⁸ M.J. Tannenbaum,⁵ P. Tarján,¹¹ J.D. Tepe,^{1,27} T.L. Thomas,³³ J. Tojo,^{24,38} H. Torii,^{24,38} R.S. Towell,¹ I. Tseruya,⁵¹ H. Tsuruoka,⁴⁸ S.K. Tuli,³ H. Tydesjö,²⁹ N. Tyurin,¹⁵ H.W. van Hecke,²⁷ J. Velkovska,^{5,44} M. Velkovsky,⁴⁴ L. Villatte,⁴⁶ A.A. Vinogradov,²³ M.A. Volkov,²³ E. Vznuzdaev,³⁷ X.R. Wang,¹³ Y. Watanabe,^{38,39} S.N. White,⁵ F.K. Wohn,¹⁶ C.L. Woody,⁵ W. Xie,⁶ Y. Yang,⁷ A. Yanovich,¹⁵ S. Yokkaichi,^{38,39} G.R. Young,³⁵ I.E. Yushmanov,²³ W.A. Zajc,^{9,†} C. Zhang,⁹ S. Zhou,^{7,51} and L. Zolin¹⁷

(PHENIX Collaboration)

¹Abilene Christian University, Abilene, TX 79699, USA

²Institute of Physics, Academia Sinica, Taipei 11529, Taiwan

³Department of Physics, Banaras Hindu University, Varanasi 221005, India

⁴Bhabha Atomic Research Centre, Bombay 400 085, India

- ⁵Brookhaven National Laboratory, Upton, NY 11973-5000, USA
⁶University of California - Riverside, Riverside, CA 92521, USA
⁷China Institute of Atomic Energy (CIAE), Beijing, People's Republic of China
⁸Center for Nuclear Study, Graduate School of Science, University of Tokyo, 7-3-1 Hongo, Bunkyo, Tokyo 113-0033, Japan
⁹Columbia University, New York, NY 10027 and Nevis Laboratories, Irvington, NY 10533, USA
¹⁰Dapnia, CEA Saclay, F-91191, Gif-sur-Yvette, France
¹¹Debrecen University, H-4010 Debrecen, Egyetem tér 1, Hungary
¹²Florida State University, Tallahassee, FL 32306, USA
¹³Georgia State University, Atlanta, GA 30303, USA
¹⁴Hiroshima University, Kagamiyama, Higashi-Hiroshima 739-8526, Japan
¹⁵Institute for High Energy Physics (IHEP), Protvino, Russia
¹⁶Iowa State University, Ames, IA 50011, USA
¹⁷Joint Institute for Nuclear Research, 141980 Dubna, Moscow Region, Russia
¹⁸KAERI, Cyclotron Application Laboratory, Seoul, South Korea
¹⁹Kangnung National University, Kangnung 210-702, South Korea
²⁰KEK, High Energy Accelerator Research Organization, Tsukuba-shi, Ibaraki-ken 305-0801, Japan
²¹KFKI Research Institute for Particle and Nuclear Physics (RMKI), H-1525 Budapest 114, POBox 49, Hungary
²²Korea University, Seoul, 136-701, Korea
²³Russian Research Center "Kurchatov Institute", Moscow, Russia
²⁴Kyoto University, Kyoto 606, Japan
²⁵Laboratoire Leprince-Ringuet, Ecole Polytechnique, CNRS-IN2P3, Route de Saclay, F-91128, Palaiseau, France
²⁶Lawrence Livermore National Laboratory, Livermore, CA 94550, USA
²⁷Los Alamos National Laboratory, Los Alamos, NM 87545, USA
²⁸LPC, Université Blaise Pascal, CNRS-IN2P3, Clermont-Fd, 63177 Aubiere Cedex, France
²⁹Department of Physics, Lund University, Box 118, SE-221 00 Lund, Sweden
³⁰Institut fuer Kernphysik, University of Muenster, D-48149 Muenster, Germany
³¹Myongji University, Yongin, Kyonggido 449-728, Korea
³²Nagasaki Institute of Applied Science, Nagasaki-shi, Nagasaki 851-0193, Japan
³³University of New Mexico, Albuquerque, NM, USA
³⁴New Mexico State University, Las Cruces, NM 88003, USA
³⁵Oak Ridge National Laboratory, Oak Ridge, TN 37831, USA
³⁶IPN-Orsay, Université Paris Sud, CNRS-IN2P3, BP1, F-91406, Orsay, France
³⁷PNPI, Petersburg Nuclear Physics Institute, Gatchina, Russia
³⁸RIKEN (The Institute of Physical and Chemical Research), Wako, Saitama 351-0198, JAPAN
³⁹RIKEN BNL Research Center, Brookhaven National Laboratory, Upton, NY 11973-5000, USA
⁴⁰St. Petersburg State Technical University, St. Petersburg, Russia
⁴¹Universidade de São Paulo, Instituto de Física, Caixa Postal 66318, São Paulo CEP05315-970, Brazil
⁴²System Electronics Laboratory, Seoul National University, Seoul, South Korea
⁴³Chemistry Department, Stony Brook University, SUNY, Stony Brook, NY 11794-3400, USA
⁴⁴Department of Physics and Astronomy, Stony Brook University, SUNY, Stony Brook, NY 11794, USA
⁴⁵SUBATECH (Ecole des Mines de Nantes, CNRS-IN2P3, Université de Nantes) BP 20722 - 44307, Nantes, France
⁴⁶University of Tennessee, Knoxville, TN 37996, USA
⁴⁷Department of Physics, Tokyo Institute of Technology, Tokyo, 152-8551, Japan
⁴⁸Institute of Physics, University of Tsukuba, Tsukuba, Ibaraki 305, Japan
⁴⁹Vanderbilt University, Nashville, TN 37235, USA
⁵⁰Waseda University, Advanced Research Institute for Science and Engineering, 17 Kikui-cho, Shinjuku-ku, Tokyo 162-0044, Japan
⁵¹Weizmann Institute, Rehovot 76100, Israel
⁵²Yonsei University, IPAP, Seoul 120-749, Korea

(Dated: October 25, 2018)

We report on the yield of protons and anti-protons, as a function of centrality and transverse momentum, in Au+Au collisions at $\sqrt{s_{NN}} = 200$ GeV measured at mid-rapidity by the PHENIX experiment at RHIC. In central collisions at intermediate transverse momenta ($1.5 < p_{\perp} < 4.5$ GeV/c) a significant fraction of all produced particles are protons and anti-protons. They show a centrality-scaling behavior different from that of pions. The \bar{p}/π and p/π ratios are enhanced compared to peripheral Au+Au, p+p and $e^{+}e^{-}$ collisions. This enhancement is limited to $p_{\perp} < 5$ GeV/c as deduced from the ratio of charged hadrons to π^0 measured in the range $1.5 < p_{\perp} < 9$ GeV/c.

PACS numbers: 25.75.Dw

Heavy-ion collisions at RHIC energies permit the study of nuclear matter at extreme energy densities. Hadrons

originating from fragmentation of partons that have undergone large momentum transfer (hard) scatterings are

sensitive probes of the hottest and densest stage of the collision. Data collected during the first RHIC run at $\sqrt{s_{NN}} = 130$ GeV led to the discovery of suppression of high transverse momentum ($p_{\perp} \geq 2$ GeV/ c) hadron production in central Au+Au collisions [1, 2, 3] when compared to expectations from nucleon-nucleon collisions. This effect, quantified in terms of a nuclear modification factor $R_{AA} = (yield_{AA}/N_{coll})/yield_{pp}$, where N_{coll} is the average number of binary nucleon-nucleon collisions, had been discussed as a possible consequence of the energy loss suffered by partons moving in a dense medium [4, 5]. Unexpectedly, it was found that R_{AA} is more strongly suppressed for π^0 than for charged hadrons [1], and that the yields of p and \bar{p} near 2 GeV/ c in central events [6] are comparable to the yield of pions ($p/\pi \sim 1$). This is in contrast to the p/π ratios of $\sim 0.1 - 0.3$, measured in $p+p$ [7] and e^+e^- [8] collisions, and to perturbative quantum chromodynamics phenomenology [9]. These results suggest that an investigation of particle composition is important for understanding the medium effect on high- p_{\perp} phenomena at RHIC. During the 2001 Au+Au run at $\sqrt{s_{NN}} = 200$ GeV the PHENIX experiment collected data to study the scaling properties of p and \bar{p} production as well as the p/π , \bar{p}/π and charged hadron to pion (h/π) ratios as a function of centrality.

The PHENIX detector [10] combines high momentum resolution with diverse particle identification (PID), resulting in hadron identification over a broad momentum range. The present results combine the measurements of π^{\pm} , p and \bar{p} with those of neutral pions [11] and inclusive charged hadrons [12]. A “minimum bias” trigger based on signals from the Beam-Beam Counters (BBC) and Zero-Degree Calorimeters (ZDC) sampled $92.2^{+2.5}_{-3.0}\%$ of the inelastic Au+Au cross-section of $\sigma_{inel}^{AuAu} = 6.9$ b [11]. The collision vertex is restricted to ± 30 cm of the nominal origin. Approximately 2×10^7 (3×10^7) minimum bias events are used in the charged (neutral) particle analysis. These samples are subdivided into 7 centrality classes based on cuts in the combined ZDC and BBC response: 0-10%, 10-20%, 20-30%, 30-40%, 40-50%, 50-60%, 60-92% of σ_{inel}^{AuAu} . The average number of participants (N_{part}) and collisions N_{coll} for each centrality class are derived from a Glauber model calculation [11].

Identified charged particles are measured over a subset of the PHENIX East-arm spectrometer covering pseudo-rapidity $|\eta| < 0.35$ and $\Delta\phi = \pi/8$ in azimuthal angle. PID is based on particle mass calculated from the measured momentum and velocity. The momentum resolution is $\delta p/p \simeq 0.7\% \oplus 1\% \times p$ (GeV/ c) and is provided by a multi-layer drift chamber (DC) followed by a multi-wire proportional chamber with pad readout (PC1). The velocity is obtained by measuring the time-of-flight (TOF) and the path length along the trajectory. The timing system uses the BBC to provide a global start signal; hits on the TOF scintillator wall, located at a radial distance of 5.06 m, provide individual stop signals. The resolution

is $\sigma \simeq 115$ ps, which allows a 4σ π/K and K/p separation up to $p_{\perp} \simeq 2$ GeV/ c and $p_{\perp} \simeq 4$ GeV/ c , respectively. A 2σ momentum dependent cut in mass squared is used up to $p_{\perp} = 2$ GeV/ c and $p_{\perp} = 4$ GeV/ c to select π and $(\bar{p})p$. Asymmetric cuts are applied at higher momenta to extend the π/K and K/p separation up to p_{\perp} of 3 and 4.5 GeV/ c . The spectra are corrected for geometrical acceptance, decay-in-flight, and reconstruction efficiency using a GEANT-based Monte Carlo (MC) simulation and embedding simulated tracks into real events with different particle multiplicities.

The p and \bar{p} yields are corrected for feed-down from weak decays using a MC simulation and the measured Λ/p and $\bar{\Lambda}/\bar{p}$ ratios at $\sqrt{s_{NN}} = 130$ GeV [13] which include contributions from Ξ and Σ^0 . Corrections for feed-down from Σ^{\pm} are not applied, but estimates based on HIJING MC give less than $\sim 5\%$ contribution. At $p_{\perp} = 0.65$ GeV/ c , about 40% of the inclusive $(\bar{p})p$ come from weak decays. This fraction reduces to $\approx 25\%$ at 4 GeV/ c . The systematic uncertainty of this correction is estimated at 6% by varying the Λ/p ($\bar{\Lambda}/\bar{p}$) ratios within the $\pm 24\%$ errors of the $\sqrt{s_{NN}} = 130$ measurement and assuming m_T -scaling at high- p_{\perp} . The above uncertainty could be larger if the Λ/p ($\bar{\Lambda}/\bar{p}$) ratios change significantly with p_{\perp} and beam energy. The additional systematic error on the overall normalization is 8% for $p_{\perp} < 3$ GeV/ c and 12% above 3 GeV/ c . Added in quadrature, the total systematic errors are 11% and 14%; the larger value is for $p_{\perp} > 3$ GeV/ c .

Inclusive charged hadrons are measured in the West-arm spectrometer covering $|\eta| < 0.35$ and $\Delta\phi = \pi/2$. Two pad chambers (PC2, PC3) located at 4.2 m and 5 m, respectively and a Ring Imaging Čerenkov Counter [12] are used to reject and subtract high- p_{\perp} background. The systematic error on the yields range from 11% for $p_{\perp} < 5$ GeV/ c to 45% at 9 GeV/ c .

Neutral pions are reconstructed via the decay $\pi^0 \rightarrow \gamma\gamma$ through an invariant mass analysis of γ pairs detected in the electromagnetic calorimeter (EMCal), which covers $\Delta\eta = 0.7$ and $\Delta\phi = \pi$. The absolute energy scale is known to $\leq 1.5\%$. The systematic errors on the π^0 spectra range from 10% to 17%, from low to high p_{\perp} [11].

Figure 1 shows the p/π and \bar{p}/π ratios as a function of p_{\perp} measured at mid-rapidity in central (0–10%), mid-central (20–30%), and peripheral (60–92%) Au+Au collisions. The open symbols represent the p/π^+ and \bar{p}/π^- measurements, while the closed symbols represent the corresponding p/π^0 and \bar{p}/π^0 ratios. The error bars are the quadratic sum of statistical errors and point-to-point systematic errors. There is an additional normalization uncertainty of $\sim 8\%$ (for p/π^+ , \bar{p}/π^-) and 12% (for p/π^0 , \bar{p}/π^0), which may shift the curves up or down, but does not affect their shapes. In the region of overlap, the π^{\pm} and π^0 measurements, with very different systematics, are consistent to within 5% to 15%. For all centralities the ratios rise steeply at low p_{\perp} and then, at a value of

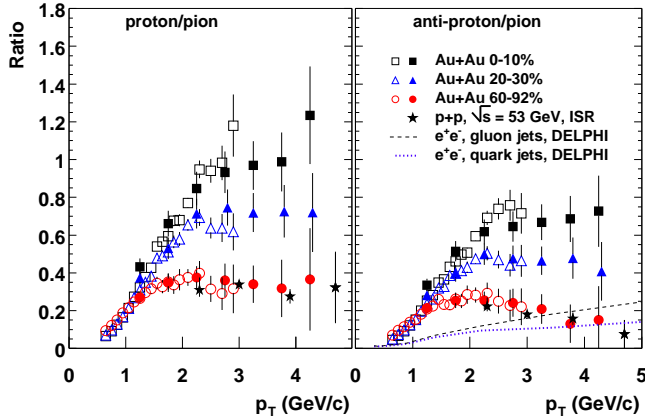


FIG. 1: p/π (left) and \bar{p}/π ratios for central(0-10%), mid-central(20-30%) and peripheral (60-92%) Au+Au collisions at $\sqrt{s_{NN}} = 200$ GeV. Open (filled) points are for π^\pm (π^0), respectively. Data from $\sqrt{s} = 53$ GeV $p+p$ collisions [7] are shown with stars. The dashed and dotted lines are $(\bar{p} + p)/(\pi^+ + \pi^-)$ ratio in gluon and in quark jets [8].

p_\perp which increases from peripheral to central collisions, level off. In central collisions the ratios are a factor of ~ 3 larger than in peripheral events. At $p_\perp > 2$ GeV/c the peripheral Au+Au data agree well with the ratios observed in $p+p$ collisions at lower energies [7] (shown with stars). The $(p + \bar{p})/(\pi^+ + \pi^-)$ ratio in gluon and quark jets produced in e^+e^- collisions [8] is shown with dashed (dotted) line. Above 3 GeV/c the p/π , \bar{p}/π ratios from peripheral collisions are also consistent with gluon and quark jet fragmentation, which should be independent of the collision system. Deviations from jet fragmentation below 3 GeV/c indicate the absence of soft hadron production in the e^+e^- data.

Hydrodynamic models have had success reproducing $(\bar{p})p$ [6, 14] and π data [6] from $\sqrt{s_{NN}} = 130$ GeV Au+Au collisions [15, 16] and preliminary 200 GeV data [17]. The calculations show good agreement with the central p, \bar{p} and π^\pm spectra up to $p_\perp \simeq 3$ and 2 GeV/c, respectively. In peripheral collisions the calculations deviate from the data above $p_\perp \simeq 1$ GeV/c. Within these models the large \bar{p}/π ratio is a natural consequence of the strong radial flow [18]. All particle spectra converge to the same slope if p_\perp is sufficiently larger than the particle mass $p_\perp \gg m_0$. The \bar{p}/π ratio is $R_{\bar{p}/\pi} \simeq 2 \exp(-\mu_b/T_{ch})$, governed only by the baryon chemical potential μ_b and the chemical freeze-out temperature T_{ch} . Using $T_{ch} = 177$ MeV and $\mu_b = 29$ MeV [19] $R_{\bar{p}/\pi}$ reaches a limiting value of 1.7. Within 10%, the same limiting behavior is expected for all centralities, since the thermal parameters vary only weakly with centrality [20]. The data are not only below the asymptotic value but also show a more pronounced centrality dependence than can be accommodated by hydrodynamics models. This suggests that other mechanisms begin to play a role before the asymptotic value is reached. At intermediate p_\perp ($2 < p_\perp < 4$ GeV/c), hard

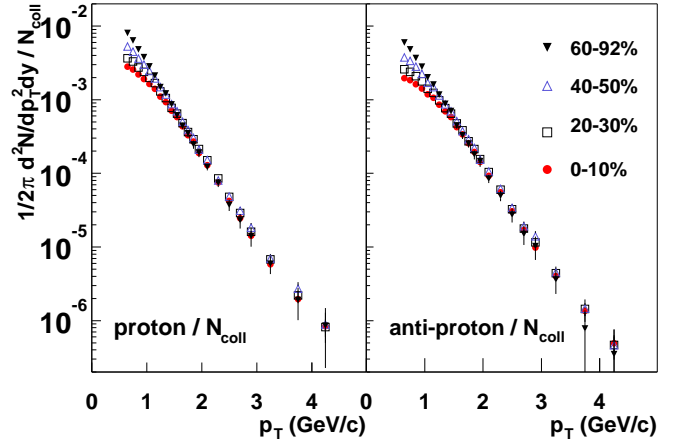


FIG. 2: p and \bar{p} invariant yields scaled by N_{coll} . Error bars are statistical. Systematic errors on N_{coll} range from $\sim 10\%$ for central to $\sim 28\%$ for 60-92% centrality. Multiplicity dependent normalization errors are $\sim 3\%$.

scattering is one possible mechanism that competes with “soft” processes as described by hydrodynamics.

Figure 2 shows the p and \bar{p} spectra for different centralities (0–10%, 20–30%, 40–50%, 60–92%) scaled by the corresponding value of N_{coll} [11]. Error bars are statistical only. Multiplicity dependent systematic errors are of the order 3%. Errors on N_{coll} range from $\sim 10\%$ for central to $\sim 28\%$ for the peripheral event class. Below $p_\perp \simeq 1.5$ GeV/c the p and \bar{p} yields scale slower than N_{coll} as expected for soft processes, and the effect of the radial flow on the shape of the spectra is clearly visible. The inverse slopes gradually increase from the most peripheral to the most central event class. Beyond $p_\perp \simeq 1.5$ GeV/c all spectra converge to the *same* slope and seem to obey N_{coll} scaling as expected for production due to hard processes in the absence of nuclear effects.

Figure 3 compares the N_{coll} scaled central to peripheral yield ratios,

$$R_{CP} = \frac{yield^{0-10\%}/N_{coll}^{0-10\%}}{yield^{60-92\%}/N_{coll}^{60-92\%}}, \quad (1)$$

for $(p + \bar{p})/2$ and π^0 . In the p_\perp range from 1.5 to 4.5 GeV/c, p and \bar{p} are not suppressed in contrast to π^0 which are reduced by a factor of 2-3. Moreover, this behavior holds for all centrality selections (Fig. 2), while the suppression in the π^0 yields increases from peripheral to central collisions [11]. The apparent scaling with N_{part} for $p_\perp \simeq 4$ GeV/c, of inclusive charged hadrons [21] which has been interpreted in terms of saturation scenario [22] appears to be somewhat coincidental, since we observe a strong species dependence not expected in the model. However, the interpretation in terms of soft and hard processes is also not straightforward. If both π and p, \bar{p} originate from the fragmentation of hard-scattered partons that lose energy in the medium, the nuclear mod-

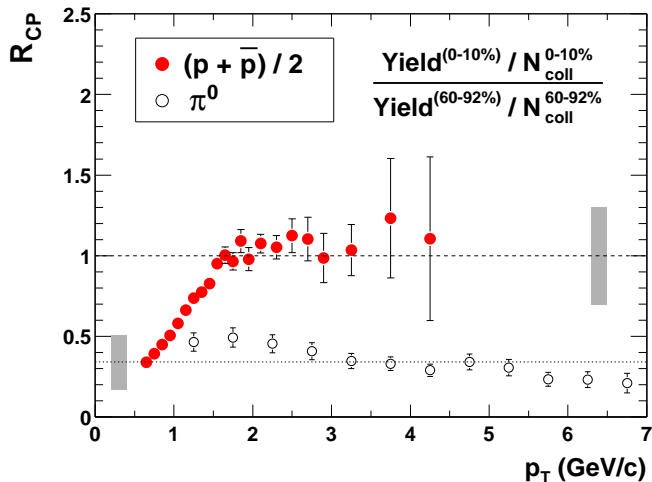


FIG. 3: Nuclear modification factor R_{CP} for $(p + \bar{p})/2$ (filled circles) and π^0 . Dashed and dotted lines indicate N_{coll} and N_{part} scaling; the shaded bars show the systematic errors on these quantities.

ification factor R_{CP} should be independent of particle species contrary to our result. As discussed above, for a “hard” description to hold, the particle ratios \bar{p}/π and p/π should reflect the fragmentation function, which favors pion production.

It is possible that nuclear effects such as the “Cronin effect” [23, 24] contribute to the observed large $(\bar{p})p/\pi$ ratios. In $p+A$ collisions at energies up to $\sqrt{s} = 38.8$ GeV a nuclear enhancement beyond N_{coll} scaling has been observed for π, K, p and their anti-particles [25]. The effect is larger for $p(\bar{p})$ than for π which leads to an enhancement of the $(\bar{p})p/\pi$ ratio compared to $p+p$ collisions. For $p+W$ the increase is a factor of ~ 2 in the range $3 < p_{\perp} < 6$ GeV/c. Theoretical descriptions assume that the effect is due to initial state scattering or p_{\perp} -broadening [26]. Recent results comparing charged hadrons to π^0 in d+Au at $\sqrt{s_{NN}} = 200$ GeV suggest that the Cronin effect in baryons is different from that in mesons [27]. Another possibility is that the variation in the p/π ratio with centrality reflects a medium-induced difference in the formation time of baryons and mesons - an effect which has been cited to explain DIS results [28].

Recently, the abundance of p relative to π in central collisions has been attributed to the recombination, rather than fragmentation, of quarks [29]. In this model, recombination for p and \bar{p} is effective up to $p_{\perp} \simeq 5$ GeV above which fragmentation dominates for all particle species. Another explanation of the observed large baryon content invokes a topological gluon configuration: the baryon junction [30]. A centrality dependence, which is in qualitative agreement with our results, has been predicted [9]. In both theoretical models, the baryon/meson enhancement is limited to $p_{\perp} < 5$ -

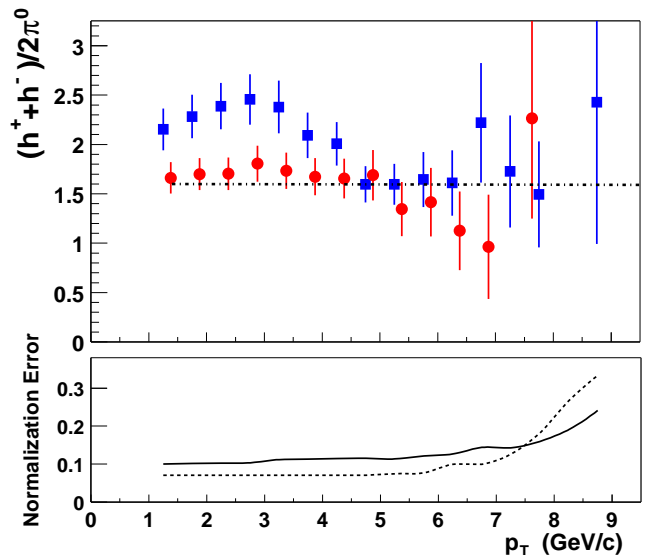


FIG. 4: Charged hadron to π^0 ratio in central (0-10% - squares) and peripheral (60-92% - circles) Au+Au collisions. The peripheral data points are offset by +130 MeV/c for clarity. The line at 1.6 is the h/π ratio measured in $p+p$ collisions [7]. The lower panel shows fractional normalization error common to both centrality selections (solid) and the relative error between the two (dashed).

6 GeV/c. The identification of charged particles beyond $p_{\perp} \approx 4.5$ GeV/c is not yet possible with the current PHENIX configuration, however the baryon content at high p_{\perp} can be tracked indirectly using the h/π^0 ratio.

Figure 4 shows h/π^0 for central and peripheral Au+Au collisions. The error bars represent the quadratic sum of statistical and point-to-point systematic errors. In peripheral Au+Au collisions, R_{h/π^0} is consistent with the measurement in $p+p$. In central collisions in the region $1 < p_{\perp} < 4.5$ GeV/c, R_{h/π^0} is enhanced by as much as 50% above the $p+p$ value. As shown in Fig. 1, this enhancement is due to a large baryon contribution. Above $p_{\perp} \simeq 5$ GeV/c, the particle composition is consistent with that measured in $p+p$ collisions. This indicates that the centrality-scaling of the p yields should become consistent with that of π at higher p_T ($\gtrsim 5$ GeV/c). Similar trends are observed in Λ and K_S^0 measurements by the STAR collaboration [31].

We have presented a systematic study of high- p_{\perp} particle composition in Au+Au collisions at $\sqrt{s_{NN}} = 200$ GeV as a function of centrality. A large p and \bar{p} contribution which increases from peripheral to central collisions is observed in the range $1.5 < p_{\perp} < 4.5$ GeV/c. In this p_{\perp} range, the p and \bar{p} yields scale with N_{coll} , as expected for hard-scattering. This is in contrast to the centrality-dependent suppression of π^0 production. The baryon enhancement with respect to π seems to be limited to transverse momenta $p_{\perp} \sim 5$ GeV/c, as deduced from the measurement of the ratio of inclusive charged hadrons to

π^0 . We conclude that π and $(\bar{p})p$ have different dominant production mechanisms for $p_{\perp} < 5 \text{ GeV}/c$.

We thank the staff of the Collider-Accelerator and Physics Departments at BNL for their vital contributions. We acknowledge support from the Department of Energy and NSF (U.S.A.), MEXT and JSPS (Japan), CNPq and FAPESP (Brazil), NSFC (China), CNRS-IN2P3 and CEA (France), BMBF, DAAD, and AvH (Germany), OTKA (Hungary), DAE and DST (India), ISF (Israel), KRF and CHEP (Korea), RMIST, RAS, and RMAE, (Russia), VR and KAW (Sweden), U.S. CRDF for the FSU, US-Hungarian NSF-OTKA-MTA, and US-Israel BSF.

* Deceased

† PHENIX Spokesperson:zajc@nevis.columbia.edu

- [1] K. Adcox *et al.*, Phys. Rev. Lett. **88**, 022301 (2002).
- [2] K. Adcox *et al.*, Phys. Lett. **B561**, 19757 (2003).
- [3] C. Adler *et al.*, Phys. Rev. Lett. **89**, 202301 (2002).
- [4] X.N. Wang and M. Gyulassy, Phys. Rev. Lett. **68**, 1480 (1992); X.N. Wang, Phys. Rev. **C58**, 2321 (1998).
- [5] M. Gyulassy and M. Plümer, Phys. Lett. **B243**, 432 (1990); R. Baier *et al.*, Phys. Lett. **B345**, 277 (1995).
- [6] K. Adcox *et al.*, Phys. Rev. Lett. **88**, 242301 (2002).
- [7] B. Alper *et al.*, Nucl. Phys. **B100**, 237-290 (1975).
- [8] P. Abreu *et al.*, Eur. Phys. J. **C17**, 207 (2000).
- [9] I. Vitev and M. Gyulassy, Phys. Rev. **C65**, 041902 (2002); I. Vitev, M. Gyulassy, P. Levai, hep-ph/0109198.
- [10] K. Adcox *et al.*, Nucl. Instrum. Methods **A499**, 469-479 (2003) and references therein.
- [11] S. S. Adler *et al.*, submitted to Phys. Rev. Lett. , nucl-ex/0304022.
- [12] J. Jia , Nucl. Phys. **A715**, 769c (2003); S. S. Adler *et al.* (to be published).
- [13] K. Adcox *et al.*, Phys. Rev. Lett. **89**, 092302 (2002).
- [14] C. Adler *et al.*, Phys. Rev. Lett. **87**, 262302 (2001).
- [15] D. Teaney *et al.*, Phys. Rev. Lett. **86**, 4783 (2001); P. Kolb *et al.*, Nucl. Phys. **A696**, 197 (2001); P. Huovinen *et al.*, Phys. Lett. **B503**, 58 (2001).
- [16] W. Broniowski and W. Florkowski Phys. Rev. **C65**, 064905 (2002); Phys. Rev. Lett. **87**, 272302 (2001).
- [17] P.F. Kolb and R. Rapp, Phys. Rev. **C67**, 044903 (2003).
- [18] U. Heinz, P. Kolb, Nucl. Phys. **A702**, 269 (2002).
- [19] P. Braun-Munzinger, D. Magestro, K. Redlich, J. Stachel, Phys. Lett. **B518**, 41 (2001).
- [20] B. Kampfer, J. Cleymans, K. Gallmeister, S. M. Wheaton, hep-ph/0204227.
- [21] B. B. Back *et al.*, nucl-ex/0302015 (to be published).
- [22] D. Kharzeev, E. Levin, L. McLerran, Phys. Lett. **B561**, 93 (2003).
- [23] J. Cronin *et al.*, Phys. Rev. **D11**, 3105 (1975).
- [24] D. Antreasyan *et al.*, Phys. Rev. **D19**, 764 (1979).
- [25] P. B. Straub *et al.* Phys. Rev. **D45**, 3030 (1992).
- [26] M. Lev, B. Petersson, Z. Phys. **C21**, 155 (83).
- [27] S. S. Adler *et al.*, Phys. Rev. Lett. **91**, 072303 (2003).
- [28] A. Airapetian *et al.*, Eur. Phys. J. **C20**, 479 (2001).
- [29] R. C. Hwa and C. B. Yang, Phys. Rev. C **67**, 034902 (2003); R. J. Fries, B. Muller, C. Nonaka and S. A. Bass, nucl-th/0301087; V. Greco, C. M. Ko and P. Levai, nucl-th/0301093.
- [30] G.C. Rossi and G. Veneziano, Nucl. Phys. **B123**, 507 (1977); D. Kharzeev, Phys. Lett. **B378**, 238 (1996); S.E. Vance, M. Gyulassy, X.-N. Wang, Phys. Lett. **B443**, 45 (1998).
- [31] J. Adams *et al.*, nucl-ex/0306007 (to be published).